UC Santa Barbara
UC Santa Barbara Previously Published Works

Title

Mono- and Mixed-Valence Tetrathiafulvalene Semiconductors (TTF)BiI

4

and (TTF)

4

BiI

6

with 1D and 0D Bismuth-Iodide Networks

Authors

Evans, Hayden A
Labram, John G
Smock, Sara R
et al.

Peer reviewed

Mono and Mixed-Valence Tetrathiafulvalene Semiconductors (TTF)BiI$_4$ and (TTF)$_4$BiI$_6$ with 1D and 0D Bismuth-Iodide Networks

Hayden A. Evans,[*,†,‡] John G. Labram,[¶] Sara R. Smock,[†] Guang Wu,[†]

Michael L. Chabinyc,[*,§,¶] Ram Seshadri,[*,‡] and Fred Wudl[*,§]

†*Department of Chemistry and Biochemistry, University of California*

Santa Barbara, California 93106, United States

‡*Materials Research Laboratory, University of California*

Santa Barbara, California 93106, United States

¶*California NanoSystems Institute, University of California*

Santa Barbara California 93106, United States

§*Materials Department, University of California*

Santa Barbara, California 93106, United States

E-mail: hevans@mrl.ucsb.edu; mchabinyc@engineering.ucsb.edu; seshadri@mrl.ucsb.edu; wudl@chem.ucsb.edu

Abstract

Two new compounds containing tetrathiafulvalene (TTF) cations with extended and discrete anions based on Bi and I are reported. The compound $(TTF)BiI_4$ comprises $[BiI_2I_{4/2}]^-$ chains of edge-shared octahedra that are interspersed with stacks of $TTF^{+\bullet}$. The compound $(TTF)_4BiI_6$ has mixed-valence stacks of TTF and $TTF^{+\bullet}$ and discrete molecules of $TTF^{+\bullet}$ separated by discrete $[BiI_6]^{-3}$ anions. The optical and electrical transport properties of these compounds are reported. Due to the mixed-valence stacks of TTF, $(TTF)_4BiI_6$ is the significantly better electrical conductor than $(TTF)BiI_4$, despite the discrete nature of the inorganic moiety.

Introduction

Hybrid organic-inorganic materials combine the easily tuned properties of designer organic compounds with functionally and chemically diverse inorganic networks. A high degree of control is possible in such systems, enabling design of materials which can exploit the benefits of the organic and inorganic components. Tetrathiafulvalene, the functional organic cation found in the title compounds, is a precursor to some of the earliest organic metals and was chosen here for its propensity to form extended $\pi - \pi$ stacks in the solid state. TTF was first reported by Wudl *et al.* in the early 1970's[1,2] and further studies have exploited the ability of TTF and its derivatives to donate electrons,[3,4] superconduct,[5] and aid magnetic communication.[6] Prior examples of TTF and TTF derivatives containing metal-halide compounds include the superconducting hybrid of bis(ethylenedithio)-tetrathiafulvalene (BEDT-TTF) with tetracyanometallates,[7] ethylenedithio-tetrathiafulvalene (EDT-TTF) compounds of Ag and Pb iodides that are metallic,[8,9] the insulating (BEDT-TTF)BiI_4,[10] and semiconducting (BEDT-TTF)$BiBr_4$ and (BEDT-TTF)$_2$[Au(i-mnt)$_2$,[11] $TTF_3(SnCl_6)$,[12] and BEDT-TTF and EDT-TTF salts with Te and I.[13] All aforementioned compounds had electrical and optical properties heavily influenced by the packing of the TTF related moiety.

Interestingly, TTF based molecular-organic frameworks (MOFs) also show structure dependent electrical properties related to how the TTF $\pi - \pi$ systems interact along the framework. Recent work by Dincă and coworkers found a direct correlation between S–S atomic distances between neighboring TTF molecules on the overall conductivity of transition metal containing MOFs.[14,15] Alternatively, there are also MOFs which incorporate electronically active organic molecules into the porous voids (rather than in the framework) to promote charge transport by coupling to the metal centers.[16–18] Recent reviews describe the general design challenges surrounding conductive MOFs,[19–21] and summarize current state-of-the-art material performance. To date, the most conducting MOF $(Cu_3(BHT)_2)$[22] has a conductivity of $1.58 \times 10^3 \, \mathrm{S \, cm^{-1}}$ which is comparable to two of the most studied organic metals, $NMP^+TCNQ^{-\bullet}$ and $TTF^{+\bullet}\text{-}TCNQ^{-\bullet}$.[23–25]

The high conductivity of $NMP^+TCNQ^{-\bullet}$ and $TTF^{+\bullet}\text{-}TCNQ^{-\bullet}$ is attributed to a back charge-transfer wherein no well-defined neutral species are seen in the crystallography of these compounds, but the properties displayed suggest the presence of some small fraction of such neutral species (due to back charge-transfer), facilitating high measured conductivities. We recently reported a monovalent TTF hybrid, similarly containing no neutral TTF (TTF^0), but only radical cations $TTF^{+\bullet}$: $(TTF)Pb_2I_5$,[26] displaying synergistic optical and electronic properties associated with back charge-transfer between the $TTF^{+\bullet}$ stacks and the extended Pb–I network. Low energy (sub 1.0 eV) optical signatures were observed in the powder optical absorption spectrum of $(TTF)Pb_2I_5$, which are usually only seen in spectra of mixed-valence TTF halide salts, and attributed to an efficient hopping charge-transfer along the mixed-valence TTF stacks.[27,28] Furthermore, $(TTF)Pb_2I_5$ also displayed conductivity much higher than related monovalent $TTF^{+\bullet}$ salts.[29] Here we report two new tetrathiafulvalene-containing hybrid compounds with Bi and I anion networks. All the TTF are monovalent in $(TTF)BiI_4$, while $(TTF)_4BiI_6$, with TTF and $TTF^{+\bullet}$, displays mixed-valence which appears to have profound implications for electrical transport; $(TTF)_4BiI_6$ is significantly the better electrical conductor. The compounds contain varying degrees

of metal-iodide and TTF$^{+\bullet}$ connectivity, providing a good comparison between hybrid monovalent and mixed-valence TTF bismuth-iodide salts. Additionally, one of the bismuth containing systems, (TTF)$_4$BiI$_6$, crystallizes in a unique structure type where monovalent TTF$^{+\bullet}$ is isolated from an extended network of neutral TTF and TTF$^{+\bullet}$. To our knowledge this is seldom seen in TTF-derivative compounds and has yet to be documented for TTF$^{+\bullet}$ compounds. We also pay close attention to the potential nature of electronic interactions between the inorganic framework and the TTF stacks in (TTF)BiI$_4$.
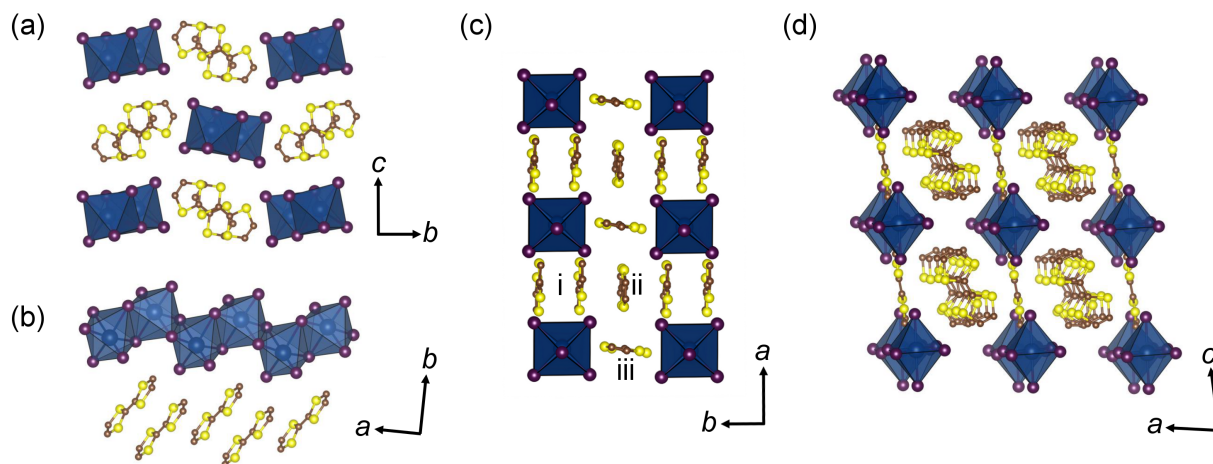
Results and Discussion

Figure 1: (a) The full structure of (TTF)BiI$_4$ looking down the a-axis, emphasizing the staggered stacks of TTF$^{+\bullet}$ dimers. (b) Alternate perspective of (TTF)BiI$_4$ looking down the c-axis, illustrating the commensurate stacking of TTF$^{+\bullet}$ dimers with edge sharing [BiI$_2$I$_{4/2}$]$^-$ chains. (c) Full crystal structure of (TTF)$_4$BiI$_6$ looking down the c-axis. This view emphasizes the mixed-valence TTF comprising alternating TTF$^{+\bullet}$ dimers (i) and neutral TTF (ii) stacked along the b-axis, as well as the alternating, isolated TTF$^{+\bullet}$ (iii) disposed normally to the a-axis. (d) Full Crystal structure of (TTF)$_4$BiI$_6$ looking down the b-axis, emphasizing the BiI$_6^{-3}$ octahedra and eclipsed nature of the mixed-valence TTF stack.

The panels of Figure 1 depict the structures of the TTF–Bi–I compounds solved from single crystal X-ray diffraction (crystallographic details in Table 1). All crystallographic representations were created using the VESTA software suite.[30] Figure 1(a) and (b) depict (TTF)BiI$_4$ projected down two different axes that allow the relative disposition of

Table 1: Crystallographic Data for (TTF)BiI$_4$ and (TTF)$_4$BiI$_6$, 296 K

	C$_6$S$_4$H$_4$BiI$_4$	C$_{24}$S$_{16}$H$_{16}$BiI$_6$
Empirical Formula	C$_6$S$_4$H$_4$BiI$_4$	C$_{24}$S$_{16}$H$_{16}$BiI$_6$
Crystal habit, color	Plate, red	Block, red
Crystal system	Monoclinic	Triclinic
Space group	Cc	$P\bar{1}$
Volume (Å^3)	3348.3(7)	1171.4(1)
a (Å)	7.6774(9)	10.237(8)
b (Å)	31.819(4)	10.460(5)
c (Å)	14.159(2)	11.166(8)
α (°)	90	84.28(1)
β (°)	104.535(2)	80.45(2)
γ (°)	90	85.85(3)
Z	8	1
ρ (g mol^{-1})	920.91	1787.71
Dens. (g cm^{-3})	3.654	2.534
Abs. (mm^{-1})	18.40	8.449
F_{000}	3192	817
Reflections (unique)	22352 (7334)	10557 (4839)
R_{int}	0.0365	0.1048
R_1	0.0357	0.0591
wR_R	0.0898	0.1347
∂F ($e\mathring{A}^{-3}$)	1.530 and -1.142	2.396 and -1.126
GOF	1.012	1.019

the TTF$^{+\bullet}$ dimer stacks and edge-shared [BiI$_2$I$_{4/2}$]$^-$ chains to be clearly distinguished. Such chains of [BiI$_2$I$_{4/2}$]$^-$ have been previously noted in the crystal structure of [BEDT-TTF]BiI$_4$.[10] It is interesting to note that the staggered TTF$^{+\bullet}$ dimer stacks are commensurate with the anionic Bi–I lattice. (TTF)BiI$_4$ is similar to the aforementioned (TTF)Pb$_2$I$_5$[26] in that both are monovalent TTF$^{+\bullet}$ salts with staggered infinite dimer stacks. However, of these two compounds, (TTF)BiI$_4$ has decreased metal-iodide connectivity (1D rather than 2D). Additionally, we note that the structure was solved in the space group Cc, and not in the higher symmetry space group $C2c$ because the two fold symmetry of the latter was not compatible with the orientation of the TTF$^{+\bullet}$ packing motif.

Figure 1(c) and (d) display different views of the structure of (TTF)$_4$BiI$_6$ and illustrate the isolated BiI$_6^{-3}$ octahedra and the unique TTF moieties: charged TTF$^{+\bullet}$ cations and neutral TTF [indicated in Figure 1(c)]. Crystallographically, neutral TTF is distinguished from TTF$^{+\bullet}$ by the shorter bond distances within and between the rings.[31] The ordered, mixed-valence TTF stacking in (TTF)$_4$BiI$_6$ is different to most other mixed-valence halide salts, where the TTF stacks are more disordered,[27,28] and furthermore, the structure type of (TTF)$_4$BiI$_6$ is quite unique due to the isolated TTF$^{+\bullet}$ seen. It is uncommon to find an discrete TTF$^{+\bullet}$ and to our knowledge is the only example of this type of TTF$^{+\bullet}$ packing. There are some similar structure types with TTF derivatives, such as (BDT-TTP)$_3$I[32] and $\alpha-$(TTM-TTP)$_2$I$_3$,[33] but these TTF derivatives pack in herringbone fashion, whereas in (TTF)$_4$BiI$_6$, the isolated TTF$^{+\bullet}$ stack perpendicular to neutral TTF, forming TTF$^{+\bullet}-$TTF^0 columns throughout the structure.

Figure 2 presents experimental and simulated electron spin resonance (ESR) spectra for polycrystalline solid state samples of (TTF)BiI$_4$ and (TTF)$_4$BiI$_6$, confirming the presence of the radical cation speacies TTF$^{+\bullet}$ in both compounds. Simulations were carried out using the EasySpin[34] code. Figure 2(a) shows the relatively easily described (TTF)BiI$_4$ spectra, simulated with three g values centered at 2.0086. The simulated spectra of (TTF)$_4$BiI$_6$ on the other hand, required eight different g tensors, potentially corresponding to the three
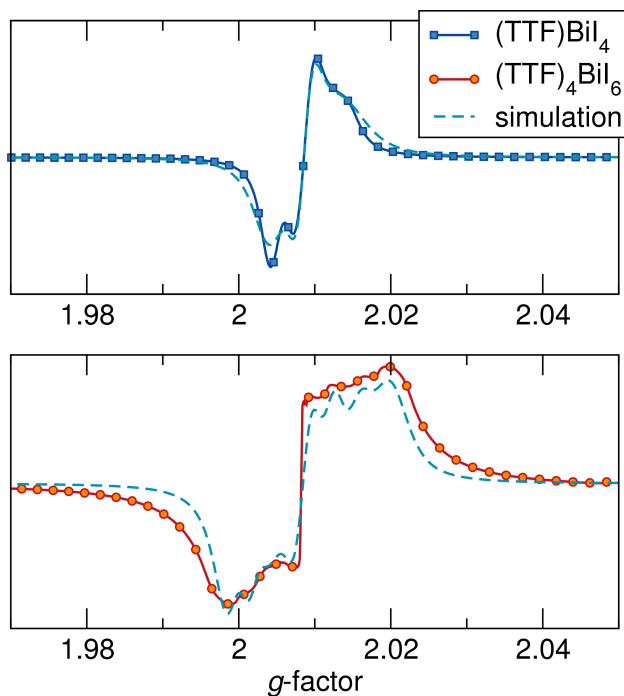
Figure 2: Solid-state room temperature ESR spectra of (a) $(TTF)BiI_4$ and (b) $(TTF)_4BiI_6$. Simulations for each are displayed as well. The g-values employed for the simulation of the spectrum for $(TTF)BiI_4$ were 2.0054, 2.0086, and 2.0111. Eight different g values: 2.0184, 2.0150, 2.0118, 2.00870, 2.0051, 2.047, 2.0010, and 1.9990 were required to simulate the spectrum of $(TTF)_4BiI_6$.

crystallographically distinct TTF$^{+\bullet}$ moieties found in the crystal structure.

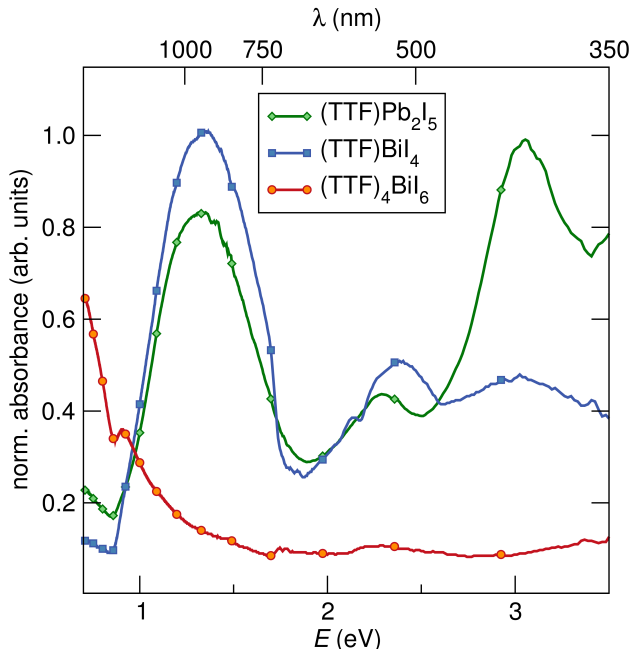Figure 3: Normalized Kubelka-Munk transformed UV-vis diffuse reflectance powder spectra of (TTF)BiI$_4$, (TTF)$_4$BiI$_6$. Data for (TTF)Pb$_2$I$_5$ are displayed for comparison.

Table 2: Assignment of diffuse reflectance optical absorption data for (TTF)BiI$_4$ and (TTF)$_4$BiI$_6$, 296 K

E (eV)	Suggested transition	(TTF)BiI$_4$	(TTF)$_4$BiI$_6$
0.70	TTF$^{+\bullet}$ + TTF^0 → TTF^0 + TTF$^{+\bullet}$	medium	strong
1.50	2 TTF$^{+\bullet}$ → TTF^0 + TTF^{2+}	strong	weak
2.30	TTF$^{+\bullet}$(dimer) → excited TTF$^{+\bullet}$(dimer)	medium	weak
3.10	TTF$^{+\bullet}$(dimer) → excited TTF$^{+\bullet}$(dimer)	medium	weak

Figure 3 displays the diffuse reflectance absorption spectra of the title compounds, as well as of the related material (TTF)Pb$_2$I$_5$, for comparison. Table 2 lists the observed peaks and previously attributed transitions.[28] The diffuse reflectance spectra show features seen in most TTF$^{+\bullet}$ salts, including absorptions peaking near 1.5 eV that has been attributed to intra-dimer charge transfer, (2TTF$^{+\bullet}$ → TTF^{+2} + neutral TTF), as well as absorptions near 2.3 eV and 3.1 eV which correspond to molecular transitions of the TTF$^{+\bullet}$.[27,28] The spectrum of (TTF)BiI$_4$ shows the strongest absorption at 1.5 eV and displays weaker absorptions at 2.3 eV, 3.0 eV, and 0.70 eV. When compared to the similarly structured (TTF)Pb$_2$I$_5$,

this increased 1.5 eV absorption in (TTF)BiI$_4$ could be due to the decreased dimer-dimer eclipsing, which prevents long range charge transfer through the stack. The powder absorption spectra of both (TTF)BiI$_4$ and (TTF)Pb$_2$I$_5$ also show absorptions below an energy of 1.0 eV. Absorptions below an energy of 1.0 eV can be attributed to charge transfer between neutral TTF and TTF$^{+\bullet}$, and are primarily seen in spectra of mixed-valence TTF salts [*eg.* (TTF)Br$_{0.71}$, (TTF)I$_{0.71}$, (TTF)SCN$_{0.57}$][27,28] and not in the spectra of monovalent salts. For the (TTF)Pb$_2$I$_5$ material, these absorptions were attributed to back charge-transfer between the TTF$^{+\bullet}$ stacks and the inorganic networks. However, one explanation for these signatures is that in most monovalent salts the dimer pairs do not pack favorably for charge transfer (herringbone fashion). In (TTF)Pb$_2$I$_5$ and (TTF)BiI$_4$ dimers are packed parallel and close enough to $\pi - \pi$ stack, which should facilitate this sub 1 eV hopping transition throughout respective TTF$^{+\bullet}$ stacks. We believe this to be part of the story for why these absorptions are seen in diffuse reflectance spectra, but as we will show, other behavior in these monovalent salts suggests back-charge transfer between the metal iodide network and TTF$^{+\bullet}$ stacks. The powder optical absorbance spectrum of (TTF)$_4$BiI$_6$ is primarily absorption in the NIR due to the presence of free carriers in the material. These NIR absorptions dwarf the interdimer and molecular TTF$^{+\bullet}$ absorptions above 1.0 eV. Absorptions below an energy of 2.1 eV in the spectra displayed here are not associated with the inorganic network. This is because most bismuth iodide systems maintain a constant band gap near or greater than 2.1 eV, regardless of metal-iodide connectivity and structure.[35]

Table 3: Single crystal NIR optical data for (TTF)BiI$_4$, 296 K

E (eV)	Suggested transition	0°	90°
0.73	TTF$^{+\bullet}$ + TTF^0 → TTF^0 + TTF$^{+\bullet}$	weak	weak
0.85	Bi-I$_m$ + TTF$^{+\bullet}$→ Bi-I$_m$ + TTF^0	strong	absent
1.15	Bi-I$_m$ + TTF$^{+\bullet}$→ Bi-I$_m$ + TTF^0	strong	medium
1.50	2 TTF$^{+\bullet}$ → TTF^0 + TTF^{2+}	strong	strong

Single crystal polarized light experiments have been performed prior with other TTF$^{+\bullet}$ containing salts as a way to isolate charge transfer absorptions parallel and perpendicular
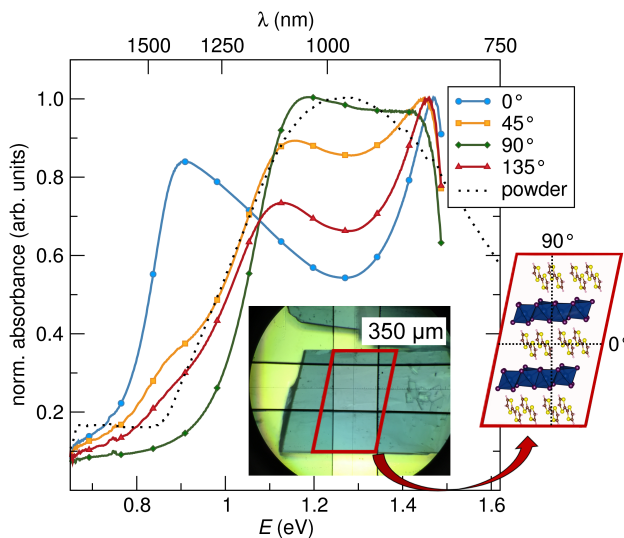
Figure 4: Kubelka-Munk transformed NIR reflectance spectra of $(TTF)BiI_4$ single crystals as well as the powder diffuse reflectance UV-vis spectrum of $(TTF)BiI_4$ from Figure 3. Polarization at zero degrees is parallel to the horizontal axis (and $TTF^{+\bullet}$ stacks), and ninety degrees is perpendicular to the horizontal axis (and $TTF^{+\bullet}$ stacks). It is interesting to note that regardless of polarization the absorption at 1.5 eV remains constant, and that the absorptions at 1.15 eV and 0.85 eV vary in intensity based on polarization. The inset displays a microscope photograph of a representative $(TTF)BiI_4$ single crystal, showing the well-developed (010) face, as well as a carton crystallographic depiction of the (010) face.

to $TTF^{+\bullet}$ containing stacks.[27,28] It was our hope that this type of experiment could provide further information on potential charge transfer occurring between the inorganic and organic networks in $(TTF)BiI_4$. Figure 4 displays room temperature single crystal NIR reflectance spectra, transformed to absorbance, as well as the powder UV-vis data for $(TTF)BiI_4$ over the same energy range. The spectra were taken at varying polarization angles between the energies 0.70 eV and 1.65 eV. Included is an inset photograph of a representative single crystal with the developed (010) face (looking down b-axis) that was used for the NIR experiment, and a crystallographic depiction of the (010) face. The 0° data is oriented parallel to the $TTF^{+\bullet}$ stacks and 90° is perpendicular to the $TTF^{+\bullet}$ stacks. The growth orientation was established with a single crystal x-ray diffractometer (included in the supporting information).

Considering each polarized $(TTF)BiI_4$ NIR spectrum in Figure 4, it is noted that all spectra have absorptions that are dependent on the angle of incident light. This is expected

10

(due to the anisotropic nature of the TTF$^{+\bullet}$ stacking), but the location and behavior of these absorptions is nontraditional for monovalent TTF$^{+\bullet}$ materials. In total, four absorption peaks are seen in all spectra with varying intensity, listed with proposed transitions in Table 3. The intensity of the peak at 1.5 eV is independent of polarization angle. In contrast, the intensity of the 1.15 eV and 0.85 eV peaks are angle dependent. The weak peak at 0.73 eV is seen with similar intensity regardless of polarization angle.

In NIR spectra of other monovalent TTF$^{+\bullet}$salts, the intensity of the 1.5 eV peak can be reduced as light is made perpendicular to TTF$^{+\bullet}$ stacks.[28] As such, because the 1.5 eV absorption appears angle independent in the single crystal absorption spectra suggests two potential explainations. One, that different charge transfer processes are present between the TTF$^{+\bullet}$dimers in (TTF)BiI$_4$, leading us to believe that the inorganic-network is maintaining localized charge-transfer between dimers regardless of incident light polarization, or two, that there is partial overlap of the spectra at 1.5 eV. Aside from the absorptions at 1.5 eV however, the peaks at 1.15 eV and 0.85 eV, as well as the peak at 0.73 eV, are quite interesting because they are usually unseen in other monovalent salt spectra. (TTF)BiI$_4$ is a monovalent TTF$^{+\bullet}$ salt, and would be expected to show similar optical properties to salts like (TTF)ClO$_4$ or (TTF)Br$_{1.0}$, but because of these sub 1.0 eV absorptions, (TTF)BiI$_4$ has optical signatures similar to a mixed-valence salt like (TTF)I$_{0.71}$.[27] Specifically, the 90° polarization spectrum shows that when light is polarized perpendicular to the TTF$^{+\bullet}$ stacks and the [BiI$_2$I$_{4/2}$]$^-$ chains, that the absorptions are primarily at 1.5 eV and 1.15 eV. In the 0° spectrum, when light is polarized parallel to the TTF$^{+\bullet}$ stacks and the [BiI$_2$I$_{4/2}$]$^-$ chains, there are absorptions primarily at 1.5 eV and 0.85 eV. The absorptions seen at 1.15 eV and 0.85 eV are hard to definitively attribute to specific transitions as they are not seen in other monovalent TTF$^{+\bullet}$ salts, but it is our assumption that they are related to two different pathways for a synergistic back charge-transfer transition related to the Bi-I network.

Figure 5(a) displays the temperature-dependence of the four-probe electrical conductivity σ on pressed pellets of (TTF)BiI$_4$ and (TTF)$_4$BiI$_6$ as a function of temperature. For
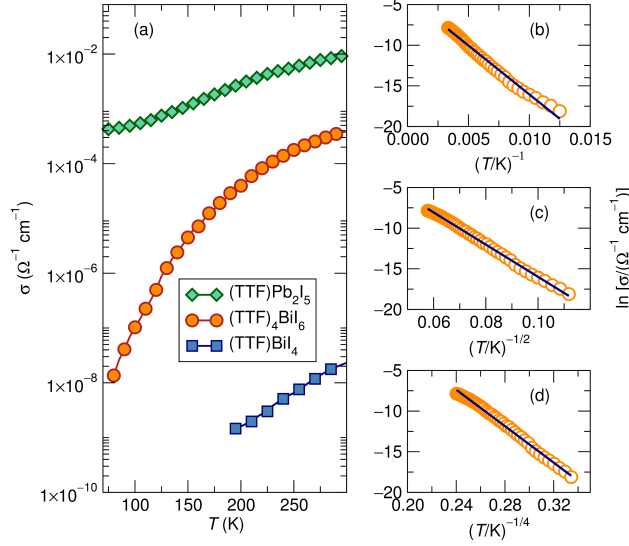
Figure 5: (a) Four probe conductivity measurements on pressed pellet samples of $(TTF)BiI_4$, $(TTF)_4BiI_6$, and $(TTF)Pb_2I_5$ (for comparison) plotted as conductivity (Ω^{-1} cm^{-1}) versus temperature. There was no detectable conductivity of $(TTF)BiI_4$ below $T = 185$ K. Activation energy fits for the conductivity data of $(TTF)_4BiI_6$ are shown in (b),(c), and (d) using Arrhenius, 1-dimensional, and 3-dimensional variable-range hopping fits, respectively. A description of the measurement as well as plots of the conductivity versus inverse temperature are included in the Supporting Information.

reference, data for the previously reported compound $(TTF)Pb_2I_5$[26] are also displayed. Neither of the samples from this study are as conductive as $(TTF)Pb_2I_5$. $(TTF)BiI_4$ is a significantly poorer electrical conductor than $(TTF)_4BiI_6$; by about 185 K, the DC conductivity of $(TTF)BiI_4$ is too low to be measured reliably. $(TTF)_4BiI_6$ in contrast, has an electrical conductivity that is close to $10^{-4}\,\Omega^{-1}$ cm^{-1} at 300 K. By 80 K, the value of the conductivity of $(TTF)_4BiI_6$ has decreased by four orders of magnitude. Attempts to fit the temperature-dependence to activated behavior [Figure 5(b)] throughout the measured temperature range proved unsatisfactory. Attempts were also made to fit the data to models of variable range hopping (VRH) following the formulation of Mott:[36] $\sigma = \sigma_0 \exp[-(T_0/T)^\nu]$. As seen from Figures 5(c) and (d), the choice of $\nu = 1/2$ appears to best fit the data, in contrast to $\nu = 1/4$, which is the more typical expectation for 3D VRH.[37] The exponent $\nu = 1/2$ could be indicative of VRH in 1D, *ie.* along the mixed-valence stack of TTF along the b crystallographic direction. An alternate explanation would involve Coulomb correlations,

12

which are also consistent with the nature of the radical species in the TTF stacks.[36]

In the compounds described above, there are several contributors to the electrical conductivity, including the connectivity of the inorganic moieties and the nature (radical cation or neutral) and stacking of the TTF species. For the two Bi-based compounds reported here, we would expect from considerations of mixed-valence of the TTF, that $(TTF)_4BiI_6$ would have the high conductivity[38] as is indeed seen. From considerations of extended connectivity of the inorganic Bi–I framework, $(TTF)BiI_4$ could potentially be a good conductor, or at least, a good semiconductor, but that is not borne out by the measurements. Perhaps the most surprising aspect is that the previously studied $(TTF)Pb_2I_5$ is so much the better conductor of all three materials considered. While $(TTF)Pb_2I_5$ has extended inorganic connectivity (like $(TTF)BiI_4$), it does not have mixed-valence stacks displayed in the structure of $(TTF)_4BiI_6$. From an electronic standpoint, $(TTF)Pb_2I_5$ most resembles $(TTF)BiI_4$, so the large differences in the electrical transport behavior are at first sight somewhat puzzling. A potential explanation, made originally to describe the properties of $(TTF)Pb_2I_5$, is that the inorganic and organic components function synergistically to give rise to the observed properties, and perhaps that is not as much the case for these Bi–I compounds.

Conclusions

We have prepared and characterized two new tetrathiafulvalene hybrid compounds with bismuth-iodide anion networks: $(TTF)BiI_4$ and $(TTF)_4BiI_6$. Both compounds are semiconductors with properties that appear to be influenced by the degree of bismuth-iodide connectivity, and by the packing and valence state of the TTF species. The optical properties of $(TTF)BiI_4$ suggest synergistic back charge-transfer similar to what has previously been reported for $(TTF)Pb_2I_5$,[26] but due to the decreased metal-iodide connectivity and the nature of the eclipsing dimers, the long range effect of the back charge-transfer is greatly

reduced. This explains why the electrical conductivity is significantly decreased; $(TTF)BiI_4$ has bulk material conductivity comparable to related monovalent salts. The compound $(TTF)_4BiI_6$ has a unique mixed-valence crystal structure comprising an isolated $TTF^{+\bullet}$ as well as mixed-valence TTF stacks, interspersed with discrete BiI_6^{-3} anions. Because of the mixed-valence TTF stacks, and despite the isolated BiI_6^{-3} anions, this compound is the significantly better electrical conductor.

Experimental

These materials were prepared in solution, similar to what has been previously reported for $(TTF)Pb_2I_5$.[26] For the preparation of $(TTF)BiI_4$, a solution of 240 mg (0.407 mmol) bismuth iodide (BiI_3, Strem 99.999%) and 75.8 mg (0.206 mmol) tetrabutylammonium iodide (TBAI, Sigma-Aldirch, 98%) was made in $2\,cm^3$ dimethylformamide (DMF anhydrous, Sigma-Aldirch) at room temperature. Once this solution was dissolved, a $3\,cm^3$ DMF solution of 60 mg (0.0762 mmol) tetrathiafulvalene fluoroborate $[(TTF)_3(BF_4)_2]$[31,39] was added drop-wise over five minutes, and allowed to stir for 15 minutes. This reaction mixture was then opened to air, layered with $5\,cm^3$ acetonitrile (MeCN) as a non-solvent, and covered. $(TTF)BiI_4$ crystallized over the course of three days and was separated from the mother liquor, washed with MeCN, and air dried. It crystallizes as black plates 0.5 mm to 1.0 mm on edge. $(TTF)_4BiI_6$ is made following the same procedure, except that 120 mg (0.203 mmol) BiI_3 is used instead. $(TTF)_4BiI_6$ crystallizes as much smaller black blocks. Both crystals appear red under a microscope when made sufficiently thin.

Single crystal x-ray diffraction data for $(TTF)BiI_4$ and $(TTF)_4BiI_6$ were collected on a Bruker KAPPA APEX II diffractometer equipped with an APEX II CCD detector using a TRIUMPH monochromator with a Mo Kα X-ray source (α = 0.71073 Å). The crystals were mounted on a cryoloop under Paratone-N oil. Absorption correction of the data was carried out using the multiscan method SADABS.[40] Subsequent calculations were carried out

using SHELXTL.[41] Structure determinations were done using direct methods. All hydrogen atom positions were omitted. Structure solution, refinement, and creation of publication materials were performed using SHELXTL. The graphical depictions used in the main paper was created with the software suite VESTA.[30]

The powder UV-vis spectra were gathered with a Shimadzu UV3600 UV-NIR Spectrometer in diffuse reflectance mode with an integrating sphere, after suspending the title compounds in $BaSO_4$ medium. These reflectance spectra were then Kubelka-Munk transformed for relative absorbance spectra. Single crystal optical experiments were conducted on multiple $(TTF)BiI_4$ crystals with a developed (010) face. The single crystals were measured on a gold substrate. The experiments were conducted using an FTIR (Vertex 70, Bruker) coupled to an infrared microscope (Hyperion 3000, Bruker). Data were collected averaging over 1,000 scans with $4\,cm^{-1}$ resolution. The microscope was operated in either spectroscopy or imaging modes (used to identify the desired single crystals). In spectroscopy mode, we performed reflection measurements where the infrared radiation was focused on the sample by a $15\times$ Cassegrain objective. The reflected light was collected by the same $15\times$ objective. A variable knife-edge aperture located in the image plane was used to define the signal collection area and only that portion of the signal was directed to the MCT detector. Typical aperture sizes were $144\,\mu m^2$ to $400\,\mu m^2$. All NIR spectra were gathered as $P_{sample}/P_{background}$, where P_{sample} is collected from an area with a single crystal was present, and $P_{background}$ was collected from an reflective adjacent area (the gold substrate) with no single crystal present.

Four-probe conductivity measurements were carried out on both compounds as a function of temperature. Pellets of $(TTF)BiI_4$ and $(TTF)_4BiI_6$ were pressed in a Carver press in a $10\,mm\times3\,mm$ rectangular pellet die under $1.2\,metric$ ton force. The dimensions of the pellets were roughly $10\,mm\times3\,mm\times1\,mm$. Further details and pictures of the pellets are provided in the supporting information. $60\,nm$ gold contacts were deposited directly onto the surface of the pellets by thermal evaporation under high vacuum (10^{-7} mbar).

The pellets were then loaded into a LakeShore cryogenic probe station and evacuated to a pressure of 10^{-4} mbar. Standard two-probe conductivity measurements were carried out at 300 K between the relevant four contacts, to access sample uniformity (details in the supporting information). The measured current was observed to be linearly proportional to the applied voltage and the average conductivity across the three regions was extracted to be $1.6(4) \times 10^{-8}$ Scm^{-1} for (TTF)BiI$_4$ and and $1.05(3) \times 10^{-4}$ S cm^{-1} for (TTF)$_4$BiI$_6$.

The conductivity was extracted by measuring the average differential resistance of the samples, between ± 1 V using a Keithley 2400 SourceMeter. The devices all had a length of 150 μm and a width of 1.25 mm. The thickness of the (TTF)BiI$_4$ and (TTF)$_4$BiI$_6$ samples were 1.00 mm and 1.20 mm respectively. Four-probe conductivity was then carried out between 300 K and 75 K using a Keithley 2400 SourceMeter and a Keithley 6220 Precision Current Source. Due to the substantial dependence of conductivity on temperature, the current range measured was varied as a function of temperature: $\pm$ 10 nA for (TTF)BiI$_4$ and ± 1 μA from 300 K to 105 K, and $\pm$ 100 nA from 100 K to 75 K for (TTF)$_4$BiI$_6$. The measured voltage was observed to be linearly proportional to the driving current for all measurements (data not shown). Below 185 K the conductivity of (TTF)BiI$_4$ was below measurable limits of the instrumentation.

Acknowledgment

guidance from Geneva Laurita.

Supporting Information

Included in the supporting information are *.cif* files, growth orientation determination for $(TTF)BiI_4$, PXRD information, and further four-probe conductivity details for the title compounds.

References

(1) Wudl, F.; Smith, G. M.; Hufnagel, E J. Unusually Stable Organic Radical. *Chem. Commun.* **1970**, 1453–1454.

(2) Wudl, F.; Wobschall, D.; Hufnagel, E. Electrical Conductivity by the bis(1,3-dithiole)-bis (1,3-dithiolium) System. *J. Am. Chem. Soc.* **1972**, *94*, 670–672.

(3) Bryce, M. R. Functionalized Tetrathiafulvalenes: New Applications as Versatile Electron Systems in Materials Chemistry. *J. Mater. Chem.* **2013**, *10*, 589–598.

(4) Martin, N. Tetrathiafulvalene: the Advent of Organic Metals. *Chem. Commun.* **2013**, *49*, 7025–7027.

(5) Crabtree, G. W.; Carlson, K. D.; Hall, L. N.; Copps, P. T.; Wang, H. H.; Emge, T. J.; Beno, M. A.; Williams, J. M. Superconductivity at Ambient Pressure in di[bis(ethyleledithio)tetrathiafulvalene]triiodide, $(BEDT)–TTF)_2I_3$. *Phys. Rev. B.* **1984**, *30*, 2958–2960.

(6) Kumai, R.; Asamitsu, A.; Tokura, Y. Magnetic and Transport Properties of Organic Radical Ion Salts Containing Tetrahalogenoferrate Anion. *Synth. Met.* **1997**, *85*, 1681–1682.

(7) Mori, T.; Kato, K.; Maruyama, Y.; Inokuchi, H. Structural and Physical Properties of a New Organic Superconductor, (BEDT–TTF)$_4$Pd(CN)$_4$H$_2$O. *Solid State Commun.* **1992**, *82*, 177–181

(8) Devic. T.; Evain, M.; Moëlo, Y.; Canadell, E.; Auban-Senzier, P.; Fourmigué, M.; Batail, P. Single Crystalline Commensurate Metallic Assemblages of π-Slabs and CdI$_2$-Type Layers: Synthesis and Properties of β-(EDT–TTF–I$_2$)$_2$[Pb$_{5/6}$□$_{1/6}$I$_2$]$_3$ and β-(EDT–TTF–I$_2$)$_2$[Pb$_{2/3+x}$Ag$_{1/3-2x}$□$_x$I$_2$]$_3$, x=0.05. *J. Am. Chem. Soc.* **2003**, *125*, 3295–3301.

(9) Devic, T.; Canadell, E.; Auban-Senzier, P.; Batail, P. (EDT–TTF–I$_2$)$_2$PbI$_3$●H$_2$O: an Ambient Pressure Metal with a β' Donor Slab Topology. *J. Mater. Chem.* **2004**, *14*, 135–137.

(10) Geiser, U.; Wang, H. H.; Budz, S. M.; Lowry, M. J.; Williams, J. M.; Ren, J.; Whangbo, M-H. Polymeric Anions Leading to Novel Packing Motifs in Donor-Radical Salts: Synthesis and Crystal and Band Electronic Structure of (BEDT–TTF)$_2$BiI$_4$. *Inorg. Chem.* **1990**, *29*, 1611–1614

(11) Bellitto, C.; Fares, V.; Federici, F.; Serino, P.; Day, P.; Kurmoo, M. Low-Dimensional Magnetic Behavior of New Radical-Ion Salts: (BEDT–TTF)$_2$[Au^{III}(i-mnt)$_2$] and (BEDT-TTF)$_2$[BiBr$_4$]. *Synth. Met.* **1996**, *79*, 33–36

(12) Kondo, K.; Matsubayashi, G.; Tanaka, T. Preparation and Properties of Tetrathiafulvalene (TTF) and Tetramethyltetraselenafulvalene Salts of Tin(IV) Halide Anions and X-Ray Crystal Structure of [TTF]$_3$[SnCl$_6$]. *J. Chem. Soc. Dalton Trans.* **1984**, *3*, 379–384.

(13) Fujiwara, M.; Tajima, N.; Imakubo; T.; Tamura, M.; Kato, R. Structural and Physical Properties of New Conducting Cation Radical Salts with Te-Based Counteranions, Tetraiodotellurate(II) and Hexaiododitellurate(II). *J. Solid State Chem.* **2002**, *168*, 396–407

(14) Narayan, T. C.; Miyakai, T.; Dincă. M. High Charge Mobility in a Tetrathiafulvalene-Based Microporous Metal-Organic Framework. *J. Am. Chem. Soc.* **2012**, *134*, 12932–12935

(15) Park, S. S.; Hontz, E. R.; Sun, L.; Hendon, C. H.; Walsh, A.; Voorhis, T. V.; Dincă. M. Cation-Dependent Intrinsic Electrical Conductivity in Isostructural Tetrathiafulvalene-Based Microporous Metal-Organic Frameworks. *J. Am. Chem. Soc.* **2015**, 8859–8862

(16) Talin, A. A.; Centrone, A.; Ford, A. C.; Foster, M. E.; Stavila, V.; Haney, P.; Kinney, R. A.; Szalai, V.; Gabaly, F. E.; Yoon, H. P.; Lonard, F.; Allendorf, M. D. Tunable Electrical Conductivity in Metal-Organic Framework Thin-Film Devices. *Science* **2014**, *343*, 66–69.

(17) Tominaka, S.; Hamoudi, H.; Suga, T.; Bennett, T. D.; Cairns, A. B.; Cheetham, A. K. Topochemical Conversion of a Dense Metal-Organic Framework from a Crystalline Insulator to an Amorphous Semiconductor. *Chem. Sci.* **2015**, *6*, 1465–1473.

(18) Beldon, P.J.; Tominaka, S.; Singh, P.; Saha Dasgupta, T.; Bithel, E. G.; Cheetham, A. K. Layered Structures and Nanosheets of Pyrimidinethiolate Coordination Polymers. *Chem. Commun.* **2014**, *50*, 3955–3957.

(19) Sun, L.; Campbell, M. G.; Dincă. M. Electrically Conductive Porous Metal-Organic Frameworks. *Angew. Chem.* **2016**, *55*, 3566–3579

(20) Allendorf, M. D.; Schwartzberg, A.; Stavila, V.; Talin, A. A. A Roadmap to Implementing Metal-Organic Frameworks in Electronic Devices: Challenges and Critical Directions. *Chem. Eur. J* **2011**, *17*, 11372–11388

(21) Stavila, V.; Talin, A. A.; Allendorf, M. D. MOF-based Electronic and Optoelectronic Devices. *Chem. Soc. Rev.* **2014**, *43*, 5994–6010.

(22) Huang, X.; Sheng, P.; Tu, Z.; Zhang, F.; Wang, J.; Geng, H.; Zou, Y.; Di, C-A.; Yi, Y.; Sun, Y.; Xu, W.; Zhu, D. A Two-Dimensional π–d Conjugated Coordination Polymer with Extremely High Electrical Conductivity and Ambipolar Transport Behaviour. *Nat. Commun.* **2015**, *6*, 7408.

(23) Torrance, J. B.; Scott B. A.; Kaufman, F. B. Optical Properties of Charge Transfer Salts of Tetracyano-quinodimethane (TCNQ). *Solid State Commun.* **1975**, *17*, 1369–1373.

(24) Tanaka, J.; Tanaka, M.; Kawai, T.; Maki, O. Electronic Spectra and Electronic Structure of TCNQ Complexes. *Bull. Chem. Soc. Jpn.* **1976**, *49*, 2358–2373

(25) Butler, M. A.; Wudl, F. Soos, Z. G. NMR Study of Partial Charge Transfer in N-methylphenazinium-tetracyanoquinodimethane (NMP-TCNQ). *Phys. Rev. B.* **1975**, *12*, 4708–4719

19

(26) Evans, H. A.; Lehner, A. J.; Labram, J. G.; Fabini, D. H.; Barreda, O.; Smock, S. R.; Wu G.; Chabinyc, M. L.; Seshadri, R.; Wudl, F. (TTF)Pb$_2$I$_5$: a Radical Cation-Stabilized Hybrid Lead Iodide with Synergistic Optoelectronic Signatures. *Chem. Mater*. **2016**, *25*, 3607–3611

(27) Sugano, T.; Yakushi, K.; Kuroda, H. Polarized Absorption Spectra of Single Crystals of Tetrathiafulvalenium Salts. *Bull. Chem. Soc. Jpn.* **1978**, *51*, 1041–1046.

(28) Torrance, J. B.; Scott, B. A.; Welber, B.; Kaufman, F. B.; Seiden, P. E. Optical Properties of the Radical Cation Tetrathiafulvalenium (TTF+) in its Mixed-Valence and Monovalence Halide Salts. *Phys. Rev. B* **1979**, 19, 730–741

(29) Scott, B. A.; LaPlaca, S, J.; Torrance, J.B., Silverman, B. D.; Welber, B. The Crystal Chemistry of Organic Metals. Composition, Structure, and Stability in the Tetrathiafulvalinium-Halide Systems. *J. Am. Chem. Soc.* **1977**, *99*, 6631–6639

(30) Momma, K.; Izumi, F. An Integrated Three-Dimensional Visualization System VESTA Using wxWidgets. *Commission on Crystallogr. Comput.* **2006**, *7*, 106–119

(31) Legros, J-P.; Bousseau, M.; Valade, L.; Cassoux, P. Crystal Structure of a Non-Conductive Non-stoichiometric Tetrathiafuvalenium Salt: (TTF)$_3$(BF$_4$)$_2$. *Mol. Cryst. Liq. Cryst.* **1983**, *100*, 181–192.

(32) Cui, H.; Otsuka, T.; Kobayashi, A.; Misaki, Y.; Kobayashi, H. Structural and Electrical Properties of Novel Molecular Conductors Based on Extended–TTF Donors BDT–TTP and I$^-$Anions. *Bull. Chem. Soc. Jpn.* **2003**, *76*, 97–102

(33) Mori, T.; Inokuchi, H.; Misaki, Y.; Yamabe, T.; Mori, H.; Tanaka, S. Crystal Structures of Highly Conducting Iodine Complexes of TTM–TTP. *Bull. Chem. Soc. Jpn.* **1994**, *67*, 661–667

(34) Stoll, S.; Schweiger, A. EasySpin, A Comprehensive Software Package for Spectral Simulation and Analysis in EPR. *J. Magn. Reson.* **2006**, *178*, 42–55.

(35) Lehner, A. J.; Fabini, D. H.; Evans, H. A.; Hebert, C.-A., Smock, S. R.; Hu, J.; Wang, H.; Zwanziger, J. W.; Chabinyc, M. L.; Seshadri, R. *Chem. Mater.* **2015**, *27*, 7137–7148.

(36) Mott, N. F. Metal–Insulator Transitions, Taylor & Francis, **1990**, pp 148.

(37) A.J. Epstein, A. J.; Lee, W.-P.; Prigodin, V. N. Low-Dimensional Variable Range Hopping in Conducting Polymers. *Synth. Met.* **2001**, *117*, 9–13

(38) Somoano, R. B.; Gupta, A.; Hadek, V. Electrical, Magnetic, and Optical Properties of the Tetrathiafulvalene (TTF) Pseudohalides, $(TTF)_{12}(SCN)_7$ and $(TTF)_{12}(SeCN)_7$ *Phys. Rev. B.* **1977**, *15*, 595–601

(39) Wudl, F.; Kaplan, M. L.; Engler, E. M.; Patel, V. V. 2,2-Bi-L,3-Dithiolylidene (Tetrathiafulvalene, TTF) and its Radical Cation Salts. *Inorg. Synth.* **1979**, *19*, 27–34.

(40) Sheldrick, G. M. *SADABS* University of Gottingen: Germany, **2005**

(41) Sheldrick, G. M. *SHELXTL PC*, Version 6.12; Bruker AXS Inc.: Madison, WI, **2005**

For Table of Contents Only
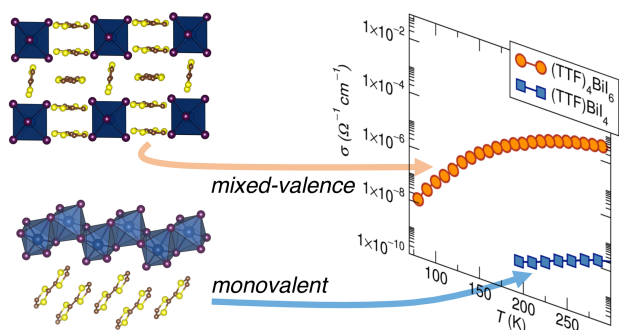
(TTF)BiI$_4$ and (TTF)$_4$BiI$_6$, whose structures are depicted here, have substantially different electrical conductivities: The latter compound is the much better electrical conductor, notwithstanding the 0D inorganic connectivity, owing to stacks of mixed valence tetrathiafulvalene. (TTF)$_4$BiI$_6$ also displays a unique crystal structure, that includes discrete molecules of TTF$^{+\bullet}$ interleaved between discrete BiI$_6^{-3}$ anions.

Supporting Information:

Mono and Mixed-Valence Tetrathiafulvalene Semiconductors, $(TTF)BiI_4$ and $(TTF)_4BiI_6$ with 1D and 0D Bismuth-Iodide Networks

Hayden A. Evans,[*,†,‡] John G. Labram,[¶] Sara R. Smock,[†] Guang Wu,[†]

Michael L. Chabinyc,[*,§,¶] Ram Seshadri,[*,‡] and Fred Wudl[*,§]

†*Department of Chemistry and Biochemistry, University of California*
Santa Barbara, California 93106, United States
‡*Materials Research Laboratory, University of California*
Santa Barbara, California 93106, United States
¶*California NanoSystems Institute, University of California*
Santa Barbara California 93106, United States
§*Materials Department, University of California*
Santa Barbara, California 93106, United States

E-mail: hevans@mrl.ucsb.edu; mchabinyc@engineering.ucsb.edu; seshadri@mrl.ucsb.edu; wudl@chem.ucsb.edu

Powder X-ray Diffraction (PXRD)

PXRD data was acquired on a Pananalytical Empyrean Powder XRD machine. PXRD data was utilized to establish bulk sample purity of isolated $(TTF)BiI_4$ and $(TTF)_4BiI_6$ over the

1

course of our experiments. We compared experimental PXRD with simulated patterns generated from single crystal x-ray diffraction data using the software suite GSAS.[1,2] The data shown in Figure S1 was performed open to air.
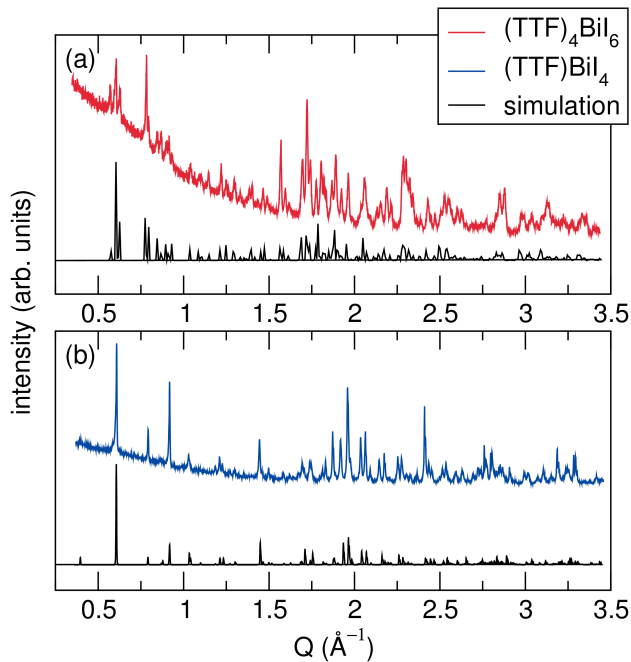

Figure S1: PXRD and simulated powder patterns for title compounds (a) $(TTF)_4BiI_6$ and (b) $(TTF)BiI_4$.

Single Crystal Growth Determination

The growth orientation of $(TTF)BiI_4$ single crystals was established on a Bruker KAPPA APEX II diffractometer equipped with an APEX II CCD detector using a TRIUMPH monochromator with a Mo Kα X-ray source (α = 0.71073 Å). The crystals were mounted on a cryoloop under Paratone-N oil. The unit cell was indexed, and using the APEX2 software suite, plane orientations established. Figure S2 is a picture taken with the APEX2 software after analysis.
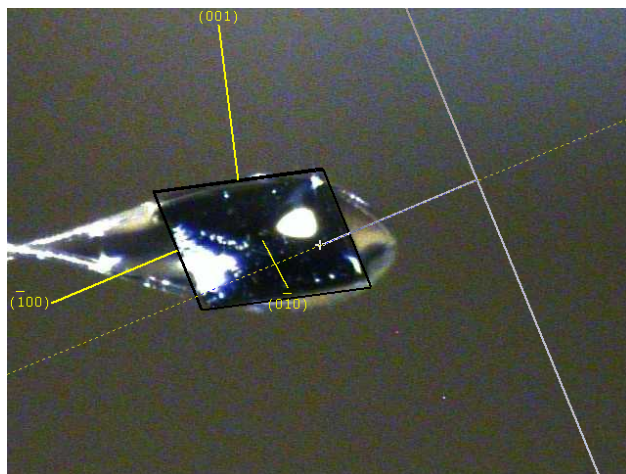
Figure S2: Photograph of (TTF)BiI$_4$ single crystal determined growth planes using APEX2 software.

Thermogravimetric Analysis (TGA)

A TA Instruments Discovery TGA was utilized for TGA of (TTF)BiI$_4$ and (TTF)$_4$BiI$_6$. A rate of 25 cm^3/min dry nitrogen purge was employed with a temperature ramp rate of 10°C/min. The maximum temperature of the experiment was 650°C. Figure S3 contains TGA data for the title compounds.
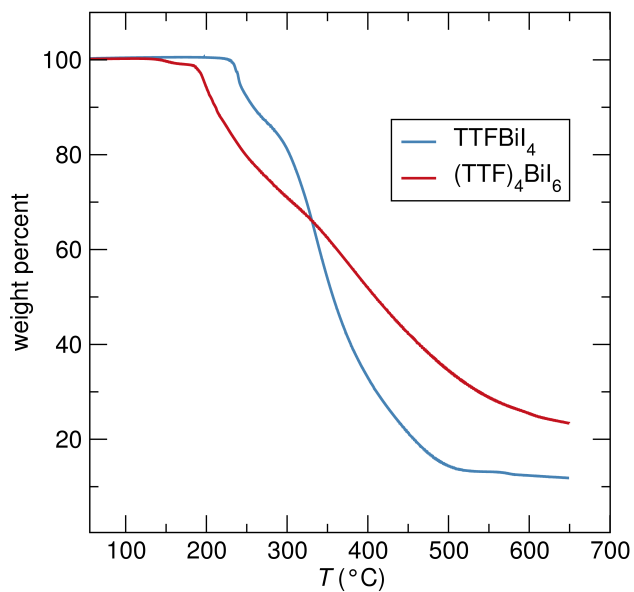
Figure S3: TGA data for the title compounds $(TTF)BiI_4$ and $(TTF)_4BiI_6$. The organic component (tetrathiafulvalene, TTF) is presumed to be the first part to degrade from $(TTF)BiI_4$ near 225°C and 141°C for $(TTF)_4BiI_6$.
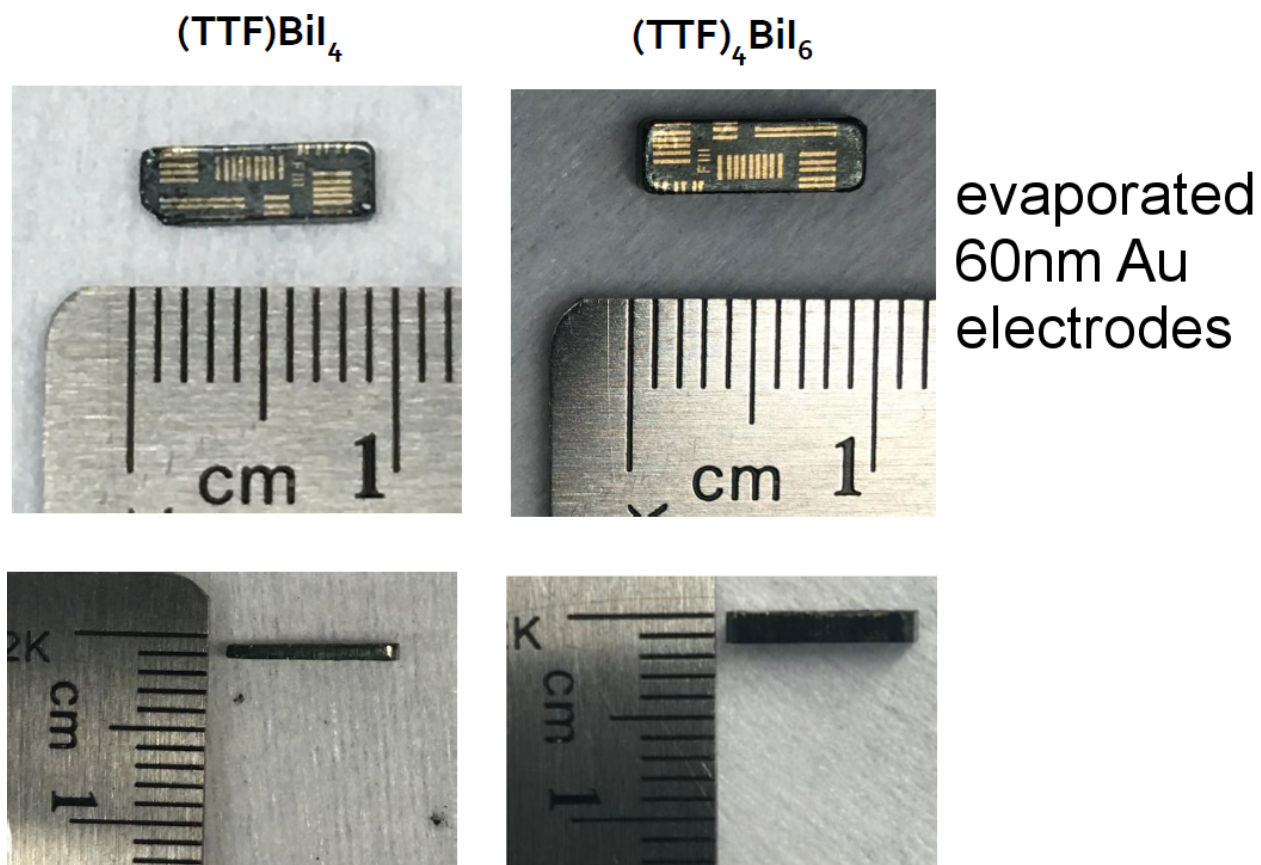
4-Probe Conductivity Measurement Setup

(TTF)BiI$_4$

(TTF)$_4$BiI$_6$

evaporated 60nm Au electrodes

Figure S4: Pictures of the pressed pellets of (TTF)BiI$_4$ and (TTF)$_4$BiI$_6$ used in the 4-probe conductivity measurements.
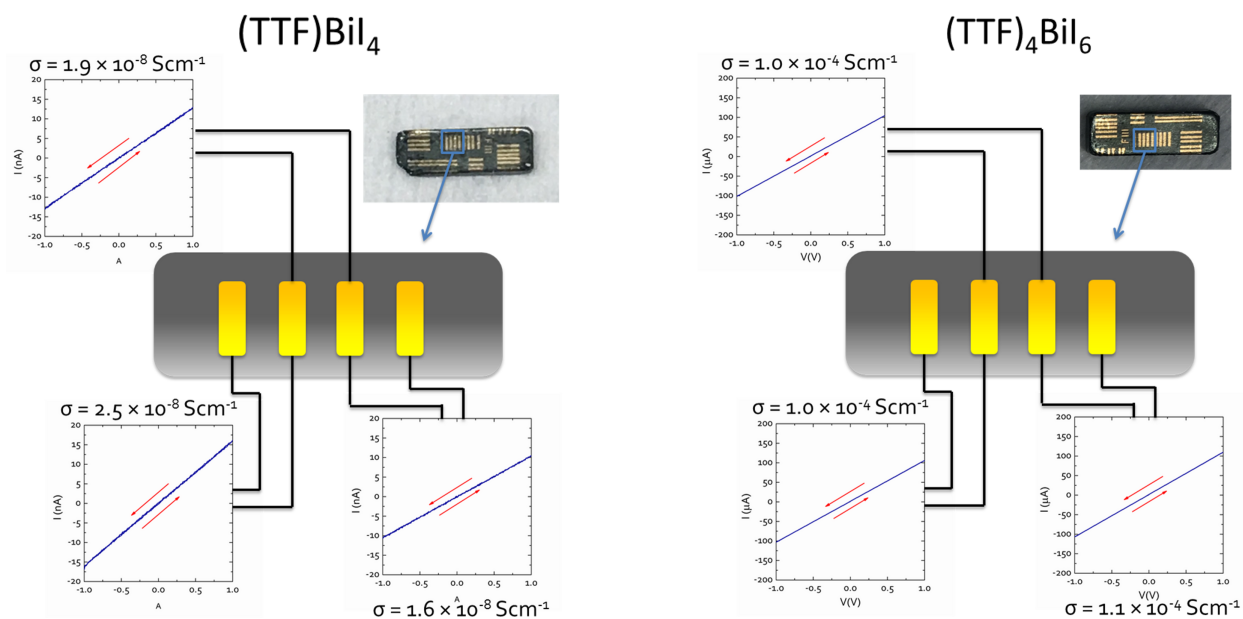
Figure S5: Photo of the pressed pellets of $(TTF)BiI_4$ and $(TTF)_4BiI_6$ that were tested, in addition to cartoon depictions of the four evaporated gold contacts used. Two probe measurements between the three near neighbor pair gold contacts are also included, verifying the consistency of four probe measurements.
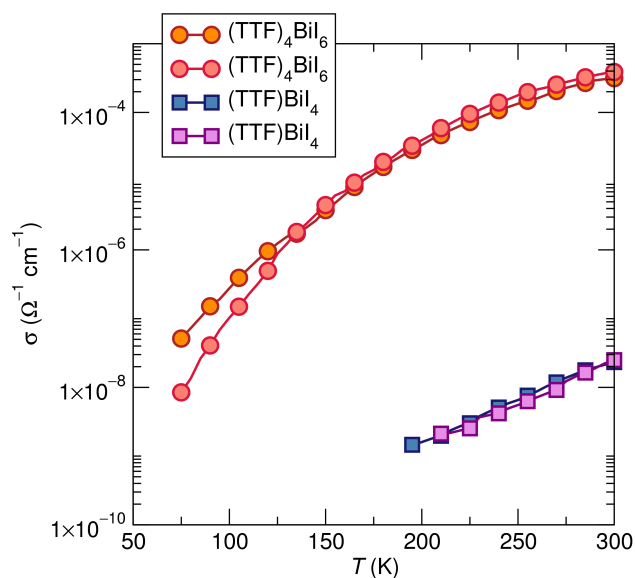

Figure S6: 4-probe conductivity pressed pellet measurements for two different batches of the title compounds. There is little variation between measurement results.
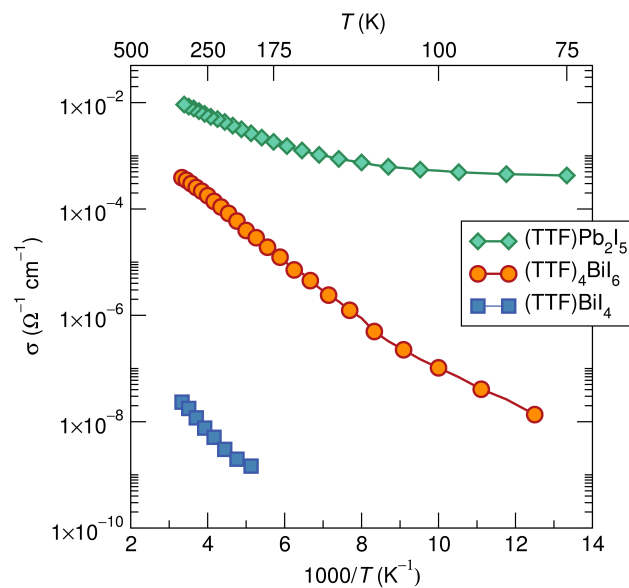
Figure S7: 4-probe conductivity data of TTF metal-halide salts, plotted with conductivity versus inverse temperature.

References

(1) Larson, A. C.; Von Dreele, R. B. "General Structure Analysis System (GSAS)", Los Alamos National Laboratory Report LAUR, **2000**, 86–748

(2) Toby, B. H. *EXPGUI*, a Graphical User Interface for GSAS. *Appl. Cryst.* **2001**, *34*, 210–213.